Published in final edited form as:
Biochemistry. 2012 June 19; 51(24): 4959–4967. doi:10.1021/bi3004473.

The aminoglycoside multi-acetylating activity of the enhanced intracellular survival (Eis) protein from *Mycobacterium smegmatis* and its inhibition

Wenjing Chen[a,b], **Keith D. Green**[a], **Oleg V. Tsodikov**[c], and **Sylvie Garneau-Tsodikova**[a,b,c,*]

Wenjing Chen: wenjing@umich.edu; Keith D. Green: kdgr@umich.edu; Oleg V. Tsodikov: olegt@umich.edu; Sylvie Garneau-Tsodikova: sylviegt@umich.edu

[a]Life Sciences Institute, 210 Washtenaw Ave, University of Michigan, Ann Arbor, MI 48109-2216

[b]Chemical Biology Doctoral Program, University of Michigan, Ann Arbor, MI 48109-2216

[c]Department of Medicinal Chemistry, University of Michigan, Ann Arbor, MI 48109-2216

Abstract

The enhanced intracellular survival (Eis) protein improves *Mycobacterium smegmatis* (*Msm*) survival in macrophages and functions as the acetyltransferase responsible for kanamycin A resistance, a hallmark of extensively drug-resistant (XDR) tuberculosis, in a large number of *Mycobacterium tuberculosis* (*Mtb*) clinical isolates. We recently demonstrated that Eis from *Mtb* (Eis_*Mtb*) efficiently multi-acetylates a variety of aminoglycoside (AG) antibiotics. Here, to gain insight into the origin of substrate selectivity of AG multi-acetylation by Eis, we analyzed AG acetylation by Eis_*Msm*, investigated its inhibition, and compared these functions to those of Eis_*Mtb*. Even though for several AGs the multi-acetylation properties of Eis_*Msm* and Eis_*Mtb* are similar, there are three major differences: (i) Eis_*Msm* di-acetylates apramycin, a conformationally constrained AG, which Eis_*Mtb* cannot modify, (ii) Eis_*Msm* tri-acetylates paromomycin, which can be only di-acetylated by Eis_*Mtb*, and (iii) Eis_*Msm* only mono-acetylates hygromycin, a structurally unique AG that is di-acetylated by Eis_*Mtb*. Several non-conserved amino acid residues lining the AG-binding pocket of Eis are likely responsible for these differences between the two Eis homologs. Specifically, we propose that because the AG-binding pocket of Eis_*Msm* is more open than that of Eis_*Mtb*, it accommodates apramycin for acetylation in Eis_*Msm*, but not in Eis_*Mtb*. We also demonstrate that inhibitors of Eis_*Mtb* that we recently discovered can inhibit Eis_*Msm* activity. These observations help define the structural origins of substrate preference among Eis homologs and suggest that Eis_*Mtb* inhibitors may be applied against all pathogenic mycobacteria to overcome AG resistance caused by Eis up-regulation.

Keywords

Acetyltransferase; Aminoglycoside antibiotics; Bacterial resistance; Enzyme promiscuity; Inhibitors; Tuberculosis

[*]Corresponding author's: sylviegt@umich.edu; Phone: 734-615-2736; Fax: 734-615-5521.

SUPPORTING INFORMATION AVAILABLE

Figures showing the multiple sequence alignment of Eis homologs from a variety of mycobacteria, structures of the Eis_*Msm* AG substrates, representative UV-Vis plots monitoring the conversion of various AGs to their acetylated products with 1 and 10 eq of AcCoA, and mass spectra of the AGs acetylated by Eis_*Msm*. This material is available free of charge via the Internet at http://pubs.acs.org.

According to the World Health Organization, over 2 billion people, about one-third of the world's population, are infected with *Mycobacterium tuberculosis* (*Mtb*) bacilli that cause the highly contagious and life-threatening tuberculosis (TB). With almost 2 million deaths and 9 million new cases each year, the TB epidemic is one of the most devastating health problems worldwide. The rapidly emerging resistance to all of the available anti-TB drugs presents one of the biggest obstacles in treating the disease. Multidrug-resistant (MDR),(1, 2) extensively drug-resistant (XDR),(3, 4) extremely drug-resistant (XXDR),(5) and more recently totally drug-resistant (TDR)(5) strains of *Mtb* have been identified.

In order to develop novel strategies to fight this notorious human pathogen, a better understanding of the basic biology of *Mtb* and its virulence is needed. While many laboratories successfully study *Mtb*, faster-dividing and non-pathogenic *Mycobacterium smegmatis* (*Msm*) has been used as a model mycobacterium to gain insight into *Mtb* mechanisms.(6–8) The entire genome of both *Mtb*(9, 10) and *Msm* have been sequenced and annotated. *Msm* shares not only more than 2,000 homologs with *Mtb* and most of the *Mtb* virulence genes, but also the same unusual cell wall structure.(7) The hyper-transformable *Msm* str. MC2 155 is now used as a convenient tool for mycobacterial genetics.

It was previously shown that up-regulation of the *Mtb* enhanced intracellular survival (Eis) protein is responsible for resistance to the aminoglycoside (AG) kanamycin A (KAN), a hallmark of XDR-TB, in a significant fraction of KAN-resistant *Mtb* clinical isolates.(11) Eis homologs have been found in many pathogens and numerous mycobacterial species (Figures 1 and S1). When transformed into *Msm*, the *eis_Mtb* gene was found to increase the intracellular survival of *Msm* in the human macrophage-like cell line U-937.(12) Based on both biochemical and structural analyses, we recently demonstrated that Eis_*Mtb* belongs to a novel family of hexameric acetyltransferases, whose tripartite fold is composed of two GCN5 *N*-acetyltransferase regions, only one of which is active, and a sterol carrier protein fold.(13) All three regions contribute to the structure of the active site and the intricate substrate-binding cavity. We showed that Eis_*Mtb* has an unprecedented ability to acetylate multiple amines of many AGs. This multi-acetylation is regio-specific; however, the substrate recognition and specificity rules for the *N*-acetylation remain unclear. Herein, in the hope that functional differences between Eis_*Mtb* and its closely genetically related, but not identical, homolog from *Msm* (Eis_*Msm*) will provide insight into the substrate recognition and *N*-acetylation specificity rules of the Eis family, we performed biochemical characterization of Eis_*Msm.* In addition, to probe the active site of Eis_*Msm*, we used AG-competitive acetylation inhibitors of Eis_*Mtb* that we recently discovered.(14)

MATERIALS AND METHODS

Bacterial Strains, Plasmids, Materials, and Instrumentation

The chemically competent *E. coli* TOP10 and BL21 (DE3) strains were purchased from Invitrogen (Carlsbad, CA). The genomic DNA from *M. smegmatis* str. MC2 155 used for PCR was a generous gift from Dr. Sabine Ehrt (Weill Cornell Medical College). The pET28a plasmid was purchased from Novagen (Gibbstown, NJ). All restriction enzymes, T4 DNA ligase, and Phusion DNA polymerase were purchased from NEB (Ipswich, MA). PCR primers were purchased from Integrated DNA Technologies (IDT; Coralville, IA). DNA sequencing was performed at the University of Michigan DNA Sequencing Core. Chemical reagents including DTNB, AcCoA, AGs (APR, AMK, HYG, KAN, NEO, SIS, SPT, STR, and RIB) (Figure S2), and chlorhexidine (**1**) were purchased from Sigma-Aldrich (Milwaukee, WI). The rest of the AGs (NEA, NET, PAR, and TOB) (Figure S2) were purchased from AK Scientific (Mountain View, CA). Compound **2** was purchased from ChemDiv Inc. (San Diego, CA). The pH was adjusted at rt. The spectrophotometric assays were performed on a multimode SpectraMax M5 plate reader using 96-well plates (Fisher

Scientific; Pittsburg, PA). Silica gel 60 F_{254} plates (Merck) were used for thin-layer chromatography (TLC) analysis. Liquid chromatography mass spectrometry (LCMS) was performed on a Shimadzu LCMS-2019EV equipped with a SPD-20AV UV-Vis detector and a LC-20AD liquid chromatograph.

Preparation of the pEis-pET28a Overexpression Constructs

The pEis_*Mtb*-pET28a plasmid encoding the Eis_*Mtb* protein was constructed as previously reported.(13) In order to prepare the pEis_*Msm*-pET28a construct, PCR was performed using *M. smegmatis* str. MC2 155 genomic DNA as a template, a forward primer 5′-TCGAGACATATGATCACGCCGCGCACCCTTC-3′, a reverse primer 5′-CCCGCGGGATCCTCAGAATCCGTATCCCAGC-3′, and Phusion DNA polymerase. The resulting amplified *eis_Msm* gene PCR fragment was inserted into the linearized pET28a via the corresponding *Nde*I/*Bam*HI restriction sites (underlined above). The plasmid encoding the Eis_*Msm* protein was transformed into *E. coli* TOP10 chemically competent cells. The plasmid bearing the *eis_Msm* gene insert was sequenced and showed perfect alignment with the reported gene sequence from *M. smegmatis* str. MC2 155 (locus tag MSMEG_3513).

Overproduction and Purification of Eis Proteins

The Eis_*Mtb* protein (with a N-terminal His_6-tag) was prepared as previously reported.(13) The overexpression and purification of the Eis_*Msm* protein was performed exactly as reported for Eis_*Mtb*.(13) Both proteins were dialyzed in Tris-HCl buffer (50 mM, pH 8.0) and stored at 4 °C. After purification, 1.1 mg of the 46,172-Da Eis_*Msm* protein was obtained per L of culture.

Determination of the AG Selectivity Profile of Eis_*Msm* by a Spectrophotometric Assay

The acetyltransferase activity of Eis_*Msm* was monitored by a UV-Vis assay in which the free thiol group of CoA, generated by the Eis_*Msm* enzyme catalyzed reaction, was allowed to react with DTNB to produce 2-nitro-5-thiobenzoate (NTB^-). The production of further ionized NTB^{2-} was monitored by increase in absorbance at 412 nm (ε_{412} = 14,150 $M^{-1}cm^{-1}$). The reaction mixtures (100 μL) containing AcCoA (0.5 mM, 5 eq), AG (0.1 mM, 1 eq), DTNB (1 mM), and Tris-HCl (50 mM, pH 8.0), were initiated by adding Eis_*Msm* (0.5 μM) at 25 °C. Reactions were monitored by taking readings every 30 s for 15 min in 96-well plate format.

Determination and Confirmation of Number of Acetylation Sites by the Spectrophotometric Assay and Mass Spectrometry

To determine the number of acetylations performed by Eis_*Msm* for a given AG, two reactions were carried out with each AG: a calibration reaction with 1 eq of AG and 1 eq of AcCoA as well as a reaction that ensured complete acetylation of the AG with 1 eq of AG and 10 eq of AcCoA. Specifically, reaction mixtures (100 μL) containing AG (0.1 mM), DTNB (1 mM), Tris-HCl (50 mM, pH 8.0), and AcCoA (0.1 mM, 1 eq or 1 mM, 10 eq), were initiated by adding Eis_*Msm* (1 μM) at 25 °C. Reactions were monitored at 412 nm as described above by taking readings every 30 s until a plateau was reached. Representative plots are shown in Figures 2A and S3. To confirm the number of acetylations on each AG substrate established by UV-Vis assays, a third reaction (20 μL) containing AG (0.67 mM, 1 eq), AcCoA (3.35 mM, 5 eq), Tris-HCl (50 mM, pH 8.0), and Eis_*Msm* protein (10 μM) was carried out overnight at 25 °C. These reactions were terminated by addition of an equal volume of ice-cold MeOH (20 μL), which was then kept at −20 °C for at least 20 min. The precipitated protein was removed by centrifugation (13,000 rpm, rt, 10 min). The masses of the acetylated AG products present in each sample were determined by LCMS in positive

mode using H_2O (0.1% formic acid) after dilution of the supernatant (10 μL) with H_2O (20 μL) and injection of all 30 μL. Mass spectra of all AGs modified by Eis_*Msm* are provided in Figures 2B and S4. A summary of the level of acetylation is presented in Table 1.

Kinetic Characterization of Eis_*Msm* Activity

The steady-state kinetic assays of acetylation of AGs (AMK, KAN, NEA, NEO, NET, PAR, SIS, and TOB) by Eis_*Msm*, were performed in two ways: (i) at a fixed concentration of AcCoA (0.1 mM) and varying concentrations of AGs (0, 31.25, 62.5, 125, 250, and 500 μM), and (ii) at a fixed concentration of each AG (0.5 mM) and varying concentrations of AcCoA (0, 16.625, 31.25, 62.5, 125, and 250 μM). All reactions were carried out in Tris-HCl (50 mM, pH 8.0) and contained AcCoA, AG, DTNB (1 mM), and Eis_*Msm* (0.25 μM). In addition, to distinguish among possible kinetic mechanisms, KAN acetylation reactions with Eis_*Msm* were carried out at AcCoA concentrations of 100, 200 and 500 μM and for each of these concentrations, at AG concentrations of 0, 20, 50, 100, 250, 500, 1000, and 2000 μM. All reactions were initiated by addition of AcCoA and performed at least in duplicate at 25 °C. As described above, the acetylation reactions were monitored at 412 nm as a function of time and absorbance readings were taken every 15–20 s. The dependence of the initial rates on the concentration of a titrant were used to calculate the apparent Michaelis-Menten kinetic parameters, $K_{m,AG}$ and $k_{cat,AG}$ (for reactions of type i above) as well as $K_{m,AcCoA}$ and $k_{cat,AcCoA}$ (for reactions of type ii), by non-linear least-squares regression data fitting with SigmaPlot (Systat Software, San Jose, CA) to the Michaelis-Menten equation. These kinetic parameters are given in Tables 2 and 3.

In order to convert these observed kinetic parameters into the mechanistic rate constants, we considered three mechanisms: 1) the random sequential mechanism, in which either AcCoA or AG can bind to free enzyme followed by binding of the other species, 2) the ordered sequential mechanism, in which AcCoA binds Eis first, followed by AG, and 3) the ordered sequential mechanism, in which AG binds Eis first, followed by AcCoA.

The random sequential mechanism is described by the following kinetic steps:

$$\begin{gathered} E+AG+AcCoA \rightleftarrows E \bullet AG+AcCoA \rightleftarrows E \bullet AG \bullet AcCoA \\ E+AG+AcCoA \rightleftarrows E \bullet AcCoA+AG \rightleftarrows E \bullet AG \bullet AcCoA \\ E \bullet AG \bullet AcCoA \rightarrow AG-Ac+CoA+E, \end{gathered} \tag{1}$$

where E is the enzyme and AG-Ac is the acetylated AG product.

Under the common simplifying assumptions of rapid AcCoA and AG binding equilibria for this mechanism, one obtains the observed kinetic parameters defined above in terms of microscopic constants:

$$k_{cat,AG} = \frac{k_{cat}[AcCoA]}{K_{d,AcCoA(E \bullet AG)} + [AcCoA]} \tag{2}$$

$$K_{m,AG} = K_{d,AG(E \bullet AcCoA)} \left(\frac{K_{d,AcCoA(E)} + [AcCoA]}{K_{d,AcCoA(E \bullet AG)} + [AcCoA]} \right) \tag{3}$$

$$k_{cat,AcCoA} = \frac{k_{cat}[AG]}{K_{d,AG(E \bullet AcCoA)} + [AG]} \tag{4}$$

$$K_{m,AcCoA}=K_{d,AcCoA(E\bullet AG)}\left(\frac{K_{d,AG(E)}+[AG]}{K_{d,AG(E\bullet AcCoA)}+[AG]}\right), \quad (5)$$

where each subscript of an equilibrium binding constant K_d designates the step in Mechanism (1); the species outside of the parentheses binds to the species in the parentheses, and k_{cat} is the microscopic rate constant of the acetylation, *i.e.* the last step in Mechanism (1).

The ordered sequential mechanism, in which only AcCoA can bind Eis first is obtained by removing the first line in Mechanism (1). For this mechanism, under the assumption of rapid equilibria, one obtains:

$$k_{cat,AG}=k_{cat} \quad (6)$$

$$K_{m,AG}=K_{d,AG}\left(1+\frac{K_{d,AcCoA}}{[AcCoA]}\right) \quad (7)$$

$$k_{cat,AcCoA}=\frac{k_{cat}[AG]}{K_{d,AG}+[AG]} \quad (8)$$

$$K_{m,AcCoA}=\frac{K_{d,AcCoA}K_{d,AG}}{K_{d,AG}+[AG]} \quad (9)$$

For the other ordered sequential mechanism, in which AG binds Eis first, we obtain by analogy:

$$k_{cat,AG}=\frac{k_{cat}[AcCoA]}{K_{d,AcCoA}+[AcCoA]} \quad (10)$$

$$K_{m,AG}=\frac{K_{d,AG}K_{d,AcCoA}}{K_{d,AcCoA}+[AcCoA]} \quad (11)$$

$$k_{cat,AcCoA}=k_{cat} \quad (12)$$

$$K_{m,AcCoA}=K_{d,AcCoA}\left(1+\frac{K_{d,AG}}{[AG]}\right) \quad (13)$$

The different functional dependences of the observed Michaelis-Menten parameters on the concentrations of AG and AcCoA for the three mechanisms allow one to distinguish among them.

For the random sequential mechanism, eqs 2–4 yield:

$$\frac{k_{cat,AG}}{K_{m,AG}k_{cat,AcCoA}} = \frac{[AcCoA]}{[AG]}\left(\frac{1}{K_{d,AcCoA(E)}+[AcCoA]}\right)\left(\frac{K_{d,AG(E\bullet AcCoA)}+[AG]}{K_{d,AG(E\bullet AcCoA)}}\right) \quad (14)$$

The left-hand side of the equality is composed of observed constants. The expression in the first parentheses on the right-hand side of the equality is constant for all AGs and, by an assumption, similar for the two Eis proteins, as explained in Results. This allows one to obtain an estimate of $K_{d,AG(E\bullet AcCoA)}$ followed by the determination of the k_{cat} from eq 4. These values are given in Table 5. Where only bounds on these values could be obtained due to a very low affinity of an AG for AcCoA-bound Eis ($K_{d,AG(E\bullet AcCoA)} \gg [AG]$), only catalytic efficiency ($k_{cat}/K_{d,AG(E\bullet AcCoA)}$) was calculated from eq 4 and reported.

Determination of Positions Acetylated on NEA by Eis_*Msm* by TLC

To establish which three positions of the NEA scaffold get acetylated by Eis_*Msm*, reactions (40 μL) were carried out at rt in Tris-HCl buffer (50 mM, pH 8.0) in the presence of AcCoA (4 mM, 5 eq), NEA (0.8 mM, 1 eq), and Eis_*Msm* (5 μM). Aliquots (4 μL) were loaded and run on a TLC plate after 0, 1, 5, 10, 30, and 120 min as well as after overnight incubation (Figure 2C). The eluent system utilized for the TLC was 3:0.8/MeOH:NH_4OH. Visualization was achieved using a cerium-molybdate stain (5 g cerium ammonium nitrate, 120 g ammonium molybdate, 80 mL H_2SO_4, 720 mL H_2O). The R_f values of the Eis_*Msm* modified NEA were consistent with those obtained for the Eis_*Mtb* reaction with NEA (Figure 2C).(13) Control reactions for mono- and di-acetylation of NEA were performed using the AG acetyltransferases AAC(2′)-Ic from *M. tuberculosis* H37Rv,(13) AAC(3)-IV from *E. coli*,(15) and AAC(6′) from the AAC(6′)/APH(2″) bifunctional enzyme individually and sequentially.(15)

Determination of Kinetic Parameters and Mode of Inhibition for Inhibitors of Eis_*Msm*

The IC_{50} values of two inhibitors, chlorhexidine (**1**) and compound **2**, were determined as previously described.(14) Briefly, the inhibitors were dissolved in Tris-HCl (50 mM, pH 8.0, containing 10% v/v DMSO) (100 μL) and 5-fold dilution series were performed. To these solutions, a mixture (50 μL) containing Eis (1 μM), NEO (400 μM), and Tris-HCl (50 mM, pH 8.0) was added and incubated at rt for 10 min. The reactions were initiated by addition of a mixture (50 μL) containing AcCoA (2 mM; ensuring that all Eis is in the AcCoA-bound form), DTNB (2 mM), and Tris-HCl (50 mM, pH 8.0). The absorbance change at 412 nm was monitored every 30 s for 15 min at 25 °C. Initial rates were calculated and the IC_{50} values were determined by using a Hill-plot analysis by using the KaleidaGraph 4.1 software (Synergy software; Reading, PA) (Figure 3).

To determine the mode of inhibition of both compounds tested, varying concentrations of NEO (final concentrations of 50, 75, 100, 150, and 200 μM) and chlorhexidine (**1**) (final concentrations of 0, 0.5, 1, 2, and 4 μM) or compound **2** (final concentrations of 0, 0.0625, 0.125, 0.25, and 0.5 μM) were used. Chlorhexidine (**1**) was found to be a competitive inhibitor of NEO whereas mixed inhibition was observed for compound **2**. The equilibrium constants K_i for chlorhexidine (**1**) binding to the Eis•AcCoA complex and constants K_i and K_i' for compound (**2**) binding to the Eis•AcCoA and Eis•AcCoA•AG complexes, respectively, were determined from the non-linear least-squares regression data fitting with SigmaPlot, to a Michaelis-Menten equation:

$$V = \frac{(1/\alpha')V_{max,AG}[AG]}{(\alpha/\alpha')K_{m,AG}+[AG]} \quad (15)$$

where V is the steady-state reaction rate, $\alpha = 1 + [I]/K_i\alpha' = 1 + [I]/K_i'$ ($\alpha' = 0$ for chlorhexidine), and $V_{max,AG}$ and $K_{m,AG}$ are the observed kinetic parameters for the reaction in the absence of inhibitor. The reaction rates were shown as Lineweaver-Burk plots (Figure 3, insets of panels A and B).

RESULTS

Substrate Specificity and Multi-acetylation Profiles of Eis Proteins

Recently, we reported the structural and biochemical characterization of Eis_*Mtb*, an AG acetyltransferase (AAC) responsible for resistance to KAN in *Mtb* clinical isolates.(13) We discovered Eis to be a novel AAC capable of unprecedented multi-acetylation of a large number of AG scaffolds. In this study, to gain insight into the unique recognition and specificity rules for the *N*-acetylation by Eis proteins, we performed a detailed characterization of AG acetylation by Eis_*Msm*, a homolog of Eis_*Mtb*, and compared its functional properties to those of Eis_*Mtb*. To ensure the validity of the comparison, we identically cloned and heterologously expressed the 46,172-Da Eis_*Msm* and the 46,597-kDa Eis_*Mtb* in *E. coli* as N-terminally His_6-tagged proteins. We first investigated the substrate specificity and the multi-acetylation profile of Eis_*Msm* by spectrophotometric assays (Table 1, Figures 2A and S3) and mass spectrometry (Figures 2B and S4). The data indicated that AMK, APR, HYG, KAN, NEA, NEO, NET, PAR, RIB, SIS, and TOB were substrates of Eis_*Msm*, whereas SPT and STR were not. We found Eis_*Mtb* and Eis_*Msm* to have generally similar AG substrate selectivity and *N*-acetylation profiles with SPT and STR not modified, KAN and NET di-acetylated, AMK, NEA, NEO, RIB, and SIS tri-acetylated, and TOB tetra-acetylated by both Eis proteins. Interestingly, we observed three major differences in the activity of these two Eis proteins: (i) Eis_*Msm* di-acetylated APR, an AG with conformationally restricted and extended cylindrical-like structure (Figures 4 and S2),(16, 17) which Eis_*Mtb* could not chemically modify, (ii) Eis_*Msm* tri-acetylated PAR, which could only be di-acetylated by Eis_*Mtb*, and (iii) Eis_*Msm* mono-acetylated HYG, a structurally unique AG that could be di-acetylated by Eis_*Mtb*. The identity of several non-conserved amino acid residues lining the AG-binding pocket of the two Eis proteins (highlighted in dark blue in Figures 1 and 4) is likely responsible for these differences in the number of acetylation sites.

Regio-specificity of Tri-acetylation of NEA by Eis Proteins

Knowing that the substrate profile for both Eis proteins was generally similar, we sought to compare the regio-specificity of their acetylating activity on an AG scaffold for which the number of sites acetylated was observed to be the same for the two proteins. We recently established by TLC and NMR spectroscopy that Eis_*Mtb* tri-acetylates NEA first at the 2′-, then at the 6′-, and finally at the 1-position.(13) Here, by using TLC and comparing the retention factor (R_f) values of the mono-, di-, and tri-acetylated NEA derivatives produced over time by Eis_*Msm* to the R_f values of their counterparts formed by Eis_*Mtb* as well as to those of mono- and di-acetylated NEA standards obtained by using individually or sequentially mono-acetylating AAC enzymes, we observed that Eis_*Msm* is also a 2′,6′,1-NEA-tri-acetylating enzyme (Figure 2C). These results suggest that AG scaffolds with the same number of acetylations by Eis_*Mtb* and Eis_*Msm* are likely modified by these two enzymes at the same positions.

Steady-state Kinetic Analysis of Eis Proteins

Seeking a deeper understanding of the subtleties differentiating Eis_*Mtb* and Eis_*Msm*, we determined the observed Michaelis-Menten catalytic parameters of steady-state acetylation for several AGs. We carried out two sets of reactions, one at a fixed concentration of AcCoA and varying concentrations of AGs (Table 2), and the other at a fixed concentration

of each AG and varying concentrations of AcCoA (Table 3). In order to convert the observed kinetic parameters into the mechanistic rate constants, we considered three kinetic mechanisms of Eis acetylation: 1) the random sequential mechanism, in which either AcCoA or AG can bind to free enzyme followed by binding of the other species, most commonly observed for other AAC enzymes (18–22), 2) the ordered sequential mechanism, in which AcCoA binds Eis only before AG does, observed for some AAC enzymes (23–25) and 3) the ordered sequential mechanism, in which AG binds Eis only before AcCoA does, not observed previously for other AAC enzymes.

To distinguish among these three mechanisms, we carried out steady-state kinetic measurements of acetylation of KAN by Eis_*Msm* at several AcCoA concentrations and for each AcCoA concentration at several KAN concentrations. For each AcCoA concentration, we obtained the [AcCoA]-dependent observed Michaelis-Menten parameters $K_{m,AG}$ and $k_{cat,AG}$ (Table 4). Each of the three mechanisms of interest is characterized by a unique dependence of these kinetic parameters on the concentration of AcCoA, as described in Materials and Methods. Notably, the random sequential mechanism is the only one of the three mechanisms for which $K_{m,AG}$ can increase with increasing [AcCoA] (for $K_{d,AcCoA(E)} < K_{d,AcCoA(E•AG)}$ in eq 3), which is what we observe (Table 4). Therefore, either ordered mechanism is inconsistent with the data. Furthermore, the dependences of $k_{cat,AG}$ and $K_{m,AG}$ on [AcCoA] agree with the random sequential mechanism described by eqs 2 and 3. Fitting the data to these two equations yields the microscopic mechanistic constants k_{cat} = 1.6 ± 0.5 s^{-1}, $K_{d,AcCoA(E•AG)}$ = 1,460 ± 600 μM, $K_{d,AG(E•AcCoA)}$ = 2,540 ± 160 μM, $K_{d,AcCoA(E)}$ = 87 ± 23 μM. Indeed, consistent with the above qualitative assessments, $K_{d,AcCoA(E)}$ is approximately 17-fold smaller than $K_{d,AcCoA(E•AG)}$. Equilibrium binding constant of AcCoA to free Eis protein ($K_{d,AcCoA(E)}$) is independent of the nature of an AG molecule. Moreover, because all the AcCoA binding residues are identical in Eis_*Msm* and Eis_*Mtb* (Figure 1), it is reasonable to assume the same value of $K_{d,AcCoA(E)}$ for both enzymes. This allows us to obtain microscopic constants k_{cat} and $K_{d,AG(E•AcCoA)}$ or their ratio for Eis_*Msm* and Eis_*Mtb* from the data in Tables 2 and 3, as explained in Materials and Methods (Table 5).

These values indicate that generally AG binds the complex of Eis with AcCoA more weakly for *Msm* than for *Mtb*. Interestingly, this weaker binding is compensated by faster catalytic rate constants k_{cat}, which results in comparable catalytic efficiencies $k_{cat}/K_{d,AG(E•AcCoA)}$ for the two proteins, irrespective of the nature of an AG substrate. For the two AGs used against *Mtb* in clinic, KAN and AMK, this effect appears to be most dramatic; they bind Eis_*Mtb*•AcCoA with much higher affinity than Eis_*Msm*, but display much higher k_{cat} values with Eis_*Msm*. Catalytic efficiencies varied in the 10–20 fold range among different AG substrates. For both Eis proteins, NET and SIS displayed the highest catalytic efficiencies among the AGs. For these two AGs, the AG affinity and k_{cat} values were similar for the two Eis homologs.

Inhibition of Eis Proteins

To further probe the differences in the active sites of Eis_*Mtb* and Eis_*Msm*, we next investigated with Eis_*Msm* the activity of the two inhibitors, chlorhexidine (**1**) and compound **2**, that we recently identified from a high-throughput screening study with Eis_*Mtb* (Figure 3).(14) We previously showed that these two Eis inhibitors display high selectivity towards the Eis_*Mtb* AG-binding site over that of any other types of AAC enzymes. Here, we found both inhibitors of Eis_*Mtb* to be effective against Eis_*Msm* in an analogous NEO acetylation assay. Interestingly, with an IC_{50} value of 1,848 ± 389 nM, chlorhexidine (**1**) appeared to be a 10-fold worse inhibitor of Eis_*Msm* than of Eis_*Mtb* (IC_{50} = 188 ± 30 nM). In contrast, with an IC_{50} value of 108 ± 19 nM, compound **2**

appeared to be a 3-fold better inhibitor of Eis_*Msm* than of Eis_*Mtb* (IC_{50} = 364 ± 32 nM). Consistently with the previously reported mode of inhibition for Eis_*Mtb*,(14) we observed that compounds **1** and **2** displayed the AG-competitive mode and the mixed mode of inhibition against NEO, respectively, when tested against Eis_*Msm*. The Michaelis-Menten analysis of the inhibition kinetics for compound **1** yields K_i values of 470 ± 150 nM for Eis_*Msm* and 105 ± 24 nM for Eis_*Mtb*, where K_i is the affinity of the inhibitor to the Eis•AcCoA complex. For compound **2**, which displays the mixed inhibition mode, K_i and K_i' values are 990 ± 520 nM and 320 ± 170 nM for Eis_*Msm* and 203 ± 47 nM and 547 ± 19 nM for Eis_*Mtb*, where K_i' is the affinity of the inhibitor to the ternary complex Eis•AcCoA•AG. Thus, this compound binds with comparable affinities to the ternary complex Eis•AcCoA•AG and to the binary complex Eis•AcCoA, for both Eis_*Msm* and Eis_*Mtb* (for either Eis protein), indicating that it does not bind directly in the AG-binding site. These results demonstrate the potential of inhibitors of Eis_*Mtb* for use against other mycobacterial species.

DISCUSSION

Eis is an *Mtb* protein whose up-regulation leads to KAN resistance, a hallmark of XDR-TB, in a large set of clinical isolates from different regions of the world.(11) With its hexameric structure and its AG multi-acetylating capabilities, Eis_*Mtb* is an AAC that is structurally and functionally highly divergent from all other characterized AACs.(13) Eis homologs are found in a number of pathogenic and non-pathogenic mycobacteria including *Mtb* and *Msm* (Figures 1 and S1). The low 10% sequence identity among Eis homologs from ten mycobacteria presented in Figure S1 may prompt one to assume that substrate recognition rules used by Eis_*Mtb* may not apply to other mycobacteria. Upon closer inspection of these sequence alignments, we find that the amino acid residues involved in CoA and AG binding as well as in catalysis are highly or even strictly conserved. Therefore, we can hypothesize that the discoveries made and information gained for Eis_*Mtb* may find application to other diseases of mycobacterial origin. In fact, the generally minor variation of the putative AG-interacting residues sets up different mycobacteria as good systems for studying the poorly understood AG-recognition rules of Eis. For several decades, *Msm* has been used as a model system to study mechanisms of *Mtb*. Eis_*Msm* and Eis_*Mtb* share 58% sequence identify (Figure 1). All amino acid residues involved in CoA binding and catalysis are strictly conserved between Eis_*Msm* and Eis_*Mtb*. However, there are four amino acid residues (highlighted in dark blue in Figures 1 and 4) in the AG-binding pockets of these two proteins that differ.

In this work we have focused on gaining a better understanding of the evolution of the novel multi-acetylation mechanism of Eis and on probing the potential application of novel Eis_*Mtb* inhibitors against other mycobacterial organisms. Our steady-state kinetic measurements indicated that Eis_*Msm*, like Eis_*Mtb*, is able to efficiently multi-acetylate many AGs and that it employs the random sequential mechanism of acetylation, similarly to the majority of other mechanistically characterized AACs.(18–22) Interestingly, the binding affinities and the catalytic rate constants differed between the two enzymes for most AGs, whereas the catalytic efficiencies were very similar. Structurally very similar NET and SIS were acetylated with the highest efficiencies among AGs for both proteins and displays comparable kinetic properties. This suggests that these two AGs must interact mostly with the features of the binding pockets that are conserved between the two enzymes. Despite the overall similarities between Eis_*Msm* and Eis_*Mtb*, we observed a major variation in the acetylating activity of APR by these two enzymes. Eis_*Msm* di-acetylated APR whereas Eis_*Mtb* did not accept APR as a substrate. APR is a structurally unique AG that contains four rings, with the two central rings fused (Figure S1). This chemical structure limits the conformational freedom of this molecule and, as a result, APR has an extended cylinder-like

conformation, as observed both in a crystalline form(16) and in solution.(17) Furthermore, this extended conformation of APR is essentially unchanged in several crystal structures of APR bound to RNA ligands.(26–28) Therefore, the AG-binding cavity of an enzyme needs to be sufficiently wide and long to accommodate a bound APR molecule for its acetylation. Because Eis_*Mtb* is unable to acetylate APR and Eis_*Msm* acetylates APR at two positions, the stiff APR scaffold serves as an excellent AG specificity discriminator between the two homologs. In order to explain this major specificity difference, we looked for structural features that could allow Eis_*Msm* to accommodate an APR molecule in the Eis_*Msm*, but not in the Eis_*Mtb* binding site. Because three out of the four primary amines of APR lie on the "terminal" rings, at least one of them is modified, which means that the AG-binding pocket should be wide and long enough to accommodate an APR cylinder with one end of it placed at the active site.

As seen in the crystal structure of Eis_*Mtb* in complex with CoA and an acetamide determined recently by our group,(13) the AG-binding cavity of Eis_*Mtb* is bifurcated, with Glu401 separating the cavity into two channels (with borders highlighted in green and in blue in Figure 4A). One channel (green) is not straight enough to fit an APR molecule without steric clashes in both Eis_*Mtb* and Eis_*Msm*. Most residues lining this channel are the same in Eis_*Mtb* and Eis_*Msm* (in Eis_*Msm* numbering in Figure 1: Phe26, Asp28, Trp38, and the carboxyl terminus denoted C-ter in Figure 4), In particular, it is not possible to avoid clashes between the APR and the catalytic carboxyl terminus, whose position is likely highly conserved,(13) and with Trp38 (Trp36 in Eis_*Mtb*). The other channel (blue) is fairly shallow in Eis_*Mtb* due to Glu401. In addition, this channel is capped at the end by Trp289 and Ile268 in Eis_*Mtb* imposing additional steric restrictions on the length of the ligand. Interestingly, all differences in the AG-binding pockets of Eis_*Mtb* and Eis_*Msm* lie in the residues that line this channel. Moreover, in Eis_*Msm*, the residues in this channel are smaller than those in Eis_*Mtb* thus likely resulting in a longer and wider channel in Eis_*Msm* than in Eis_*Mtb* and creating a cavity large enough to bind an APR molecule in a proper orientation for acetylation (Figure 4B). Specifically, Trp289 in Eis_*Mtb* is changed to an alanine (Ala287 in Eis_*Msm*) and Ile268 and Glu401 in Eis_*Mtb* to glycines (Gly266 and Gly401 in Eis_*Msm*), respectively (Figures 1 and 4). In addition, another residue lining this channel, Gln291 in Eis_*Mtb* is replaced by a smaller alanine (Ala289 in Eis_*Msm*) contributing to the channel widening. An APR molecule readily fits into this channel in the model of an Eis_*Msm* structure (Figure 4B). Even though the structural details of binding of APR to Eis_*Msm* may not all be accurately represented by this model, when taken together, our biochemical results and these structural considerations suggest that APR binding occurs in this channel.

Finally, by demonstrating that inhibitors of Eis_*Mtb* can also prevent acetylation of NEO by Eis_*Msm*, we showed that the Eis_*Mtb* inhibitory properties of these compounds could potentially be extended to other mycobacteria. As we demonstrated, the inhibitory power of each compound was somewhat different between the two mycobacteria, suggesting that these inhibitors would display varying potency among mycobacteria. Further investigations are currently underway in our laboratory to determine appropriate inhibitor-mycobacterium pairs. In the future, testing the activity of these inhibitors against other Eis-containing pathogenic bacteria to evaluate the extent of the application of these molecules will be of interest.

Supplementary Material

Refer to Web version on PubMed Central for supplementary material.

Acknowledgments

FUNDING SOURCE STATEMENT

Funding support for this work was from the Life Sciences Institute (S.G.-T.) and the College of Pharmacy at the University of Michigan (S.G.-T. and O.V.T), the National Institutes of Health (NIH) Grant AI090048 (S.G.-T.), and a grant from the Firland Foundation (S.G.-T.).

We thank Prof. Sabine Ehrt for the gift of the *M. smegmatis* str. MC2 155 genomic DNA (Weill Cornell Medical College).

ABBREVIATIONS

AcCoA	acetyl-coenzyme A
AMK	amikacin
AG	aminoglycoside
AAC	aminoglycoside acetyltransferase
APH	aminoglycoside phosphotransferase
APR	apramycin
DTNB	5,5′-dithiobis-(2-nitrobenzoic acid)
Eis	enhanced intracellular survival
eq	equivalent or equation (depending on the context)
HYG	hygromycin
KAN	kanamycin A
LCMS	liquid chromatography mass spectrometry
Msm	*Mycobacterium smegmatis*
Mtb	*Mycobacterium tuberculosis*
NEA	neamine
NEO	neomycin B
NET	netilmicin
PAR	paromomycin
RIB	ribostamycin
rt	room temperature
SIS	sisomicin
SPT	spectinomycin
STR	streptomycin
TLC	thin-layer chromatography
TOB	tobramycin
TB	tuberculosis

References

1. Caminero JA. Treatment of multidrug-resistant tuberculosis: evidence and controversies. Int J Tuberc Lung Dis. 2006; 10:829–837. [PubMed: 16898365]

2. Chan ED, Laurel V, Strand MJ, Chan JF, Huynh ML, Goble M, Iseman MD. Treatment and outcome analysis of 205 patients with multidrug-resistant tuberculosis. Am J Respir Crit Care Med. 2004; 169:1103–1109. [PubMed: 14742301]
3. Ellner JJ. The emergence of extensively drug-resistant tuberculosis: a global health crisis requiring new interventions: part I: the origins and nature of the problem. Clin Transl Sci. 2008; 1:249–254. [PubMed: 20443856]
4. Banerjee R, Schecter GF, Flood J, Porco TC. Extensively drug-resistant tuberculosis: new strains, new challenges. Expert Rev Anti Infect Ther. 2008; 6:713–724. [PubMed: 18847407]
5. Udwadia ZF, Amale RA, Ajbani KK, Rodrigues C. Totally drug-resistant tuberculosis in India. Clin Infect Dis. 2012; 54:579–581. [PubMed: 22190562]
6. Shiloh MU, DiGiuseppe Champion PA. To catch a killer. What can mycobacterial models teach us about Mycobacterium tuberculosis pathogenesis? Curr Opin Microbiol. 2010; 13:86–92. [PubMed: 20036184]
7. Reyrat JM, Kahn D. Mycobacterium smegmatis: an absurd model for tuberculosis? Trends Microbiol. 2001; 9:472–474. [PubMed: 11597444]
8. Tyagi JS, Sharma D. Mycobacterium smegmatis and tuberculosis. Trends Microbiol. 2002; 10:68–69. [PubMed: 11827806]
9. Cole ST, Brosch R, Parkhill J, Garnier T, Churcher C, Harris D, Gordon SV, Eiglmeier K, Gas S, Barry CE 3rd, Tekaia F, Badcock K, Basham D, Brown D, Chillingworth T, Connor R, Davies R, Devlin K, Feltwell T, Gentles S, Hamlin N, Holroyd S, Hornsby T, Jagels K, Krogh A, McLean J, Moule S, Murphy L, Oliver K, Osborne J, Quail MA, Rajandream MA, Rogers J, Rutter S, Seeger K, Skelton J, Squares R, Squares S, Sulston JE, Taylor K, Whitehead S, Barrell BG. Deciphering the biology of Mycobacterium tuberculosis from the complete genome sequence. Nature. 1998; 393:537–544. [PubMed: 9634230]
10. Fleischmann RD, Alland D, Eisen JA, Carpenter L, White O, Peterson J, DeBoy R, Dodson R, Gwinn M, Haft D, Hickey E, Kolonay JF, Nelson WC, Umayam LA, Ermolaeva M, Salzberg SL, Delcher A, Utterback T, Weidman J, Khouri H, Gill J, Mikula A, Bishai W, Jacobs WR Jr, Venter JC, Fraser CM. Whole-genome comparison of Mycobacterium tuberculosis clinical and laboratory strains. J Bacteriol. 2002; 184:5479–5490. [PubMed: 12218036]
11. Zaunbrecher MA, Sikes RD Jr, Metchock B, Shinnick TM, Posey JE. Overexpression of the chromosomally encoded aminoglycoside acetyltransferase eis confers kanamycin resistance in Mycobacterium tuberculosis. Proc Natl Acad Sci U S A. 2009; 106:20004–20009. [PubMed: 19906990]
12. Wei J, Dahl JL, Moulder JW, Roberts EA, O'Gaora P, Young DB, Friedman RL. Identification of a Mycobacterium tuberculosis gene that enhances mycobacterial survival in macrophages. J Bacteriol. 2000; 182:377–384. [PubMed: 10629183]
13. Chen W, Biswas T, Porter VR, Tsodikov OV, Garneau-Tsodikova S. Unusual regioversatility of acetyltransferase Eis, a cause of drug resistance in XDR-TB. Proc Natl Acad Sci U S A. 2011; 108:9804–9808. [PubMed: 21628583]
14. Green KD, Chen W, Garneau-Tsodikova S. Identification and characterization of inhibitors of the aminoglycoside resistance acetyltransferase Eis from Mycobacterium tuberculosis. ChemMedChem. 2012; 7:73–77. [PubMed: 21898832]
15. Green KD, Chen W, Houghton JL, Fridman M, Garneau-Tsodikova S. Exploring the substrate promiscuity of drug-modifying enzymes for the chemoenzymatic generation of N-acylated aminoglycosides. ChemBioChem. 2010; 11:119–126. [PubMed: 19899089]
16. O'Connor S, Lam LKT, Jones ND, Chaney MO. Apramycin, a unique aminocyclitol antibiotic. J Org Chem. 1976; 41:2087–2092. [PubMed: 932851]
17. Szilágyi L, Pusztahelyi ZS. Apramycin: Complete 1H and 13C NMR assignments and study of the solution conformation by ROESY measurements. Magn Res Chem. 1992; 30:107–117.
18. Williams JW, Northrop DB. Kinetic mechanisms of gentamicin acetyltransferase I. Antibiotic-dependent shift from rapid to nonrapid equilibrium random mechanisms. J Biol Chem. 1978; 253:5902–5907. [PubMed: 681327]

19. Magnet S, Lambert T, Courvalin P, Blanchard JS. Kinetic and mutagenic characterization of the chromosomally encoded Salmonella enterica AAC(6′)-Iy aminoglycoside N-acetyltransferase. Biochemistry. 2001; 40:3700–3709. [PubMed: 11297438]

20. Magalhaes ML, Blanchard JS. The kinetic mechanism of AAC3-IV aminoglycoside acetyltransferase from Escherichia coli. Biochemistry. 2005; 44:16275–16283. [PubMed: 16331988]

21. Martel A, Masson M, Moreau N, Le Goffic F. Kinetic studies of aminoglycoside acetyltransferase and phosphotransferase from Staphylococcus aureus RPAL. Relationship between the two activities. Eur J Biochem. 1983; 133:515–521. [PubMed: 6305650]

22. Hegde SS, Javid-Majd F, Blanchard JS. Overexpression and mechanistic analysis of chromosomally encoded aminoglycoside 2′-N-acetyltransferase (AAC(2′)-Ic) from Mycobacterium tuberculosis. J Biol Chem. 2001; 276:45876–45881. [PubMed: 11590162]

23. Kim C, Villegas-Estrada A, Hesek D, Mobashery S. Mechanistic characterization of the bifunctional aminoglycoside-modifying enzyme AAC(3)-Ib/AAC(6′)-Ib′ from Pseudomonas aeruginosa. Biochemistry. 2007; 46:5270–5282. [PubMed: 17417880]

24. Kim C, Hesek D, Zajicek J, Vakulenko SB, Mobashery S. Characterization of the bifunctional aminoglycoside-modifying enzyme ANT(3″)-Ii/AAC(6′)-IId from Serratia marcescens. Biochemistry. 2006; 45:8368–8377. [PubMed: 16819836]

25. Draker KA, Northrop DB, Wright GD. Kinetic mechanism of the GCN5-related chromosomal aminoglycoside acetyltransferase AAC(6′)-Ii from Enterococcus faecium: evidence of dimer subunit cooperativity. Biochemistry. 2003; 42:6565–6574. [PubMed: 12767240]

26. Han Q, Zhao Q, Fish S, Simonsen KB, Vourloumis D, Froelich JM, Wall D, Hermann T. Molecular recognition by glycoside pseudo base pairs and triples in an apramycin-RNA complex. Angew Chem Int Ed Engl. 2005; 44:2694–2700. [PubMed: 15849690]

27. Hermann T, Tereshko V, Skripkin E, Patel DJ. Apramycin recognition by the human ribosomal decoding site. Blood Cells Mol Dis. 2007; 38:193–198. [PubMed: 17258916]

28. Kondo J, Francois B, Urzhumtsev A, Westhof E. Crystal structure of the Homo sapiens cytoplasmic ribosomal decoding site complexed with apramycin. Angew Chem Int Ed Engl. 2006; 45:3310–3314. [PubMed: 16596680]

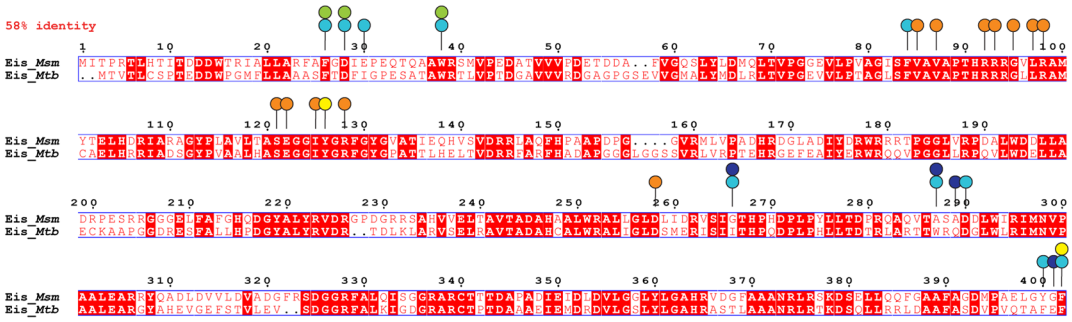

Figure 1.

Sequence alignment of Eis_*Msm* from *M. smegmatis* str. MC2 155 and Eis_*Mtb* from *M. tuberculosis* H37Rv. The two Eis homologs exhibit 58% sequence identity. Based on structural and mutagenesis studies of Eis_*Mtb*, the residues proposed to be involved in catalysis, in binding CoA, and in formation of the AG-binding pocket are marked by yellow, orange, and turquoise circles, respectively.(13) Non-conserved residues in the AG-binding pockets of these two proteins are additionally marked by dark blue circles. Conserved residues in the AG-binding pockets of Eis_*Msm* and Eis_*Mtb* are marked by green circles.

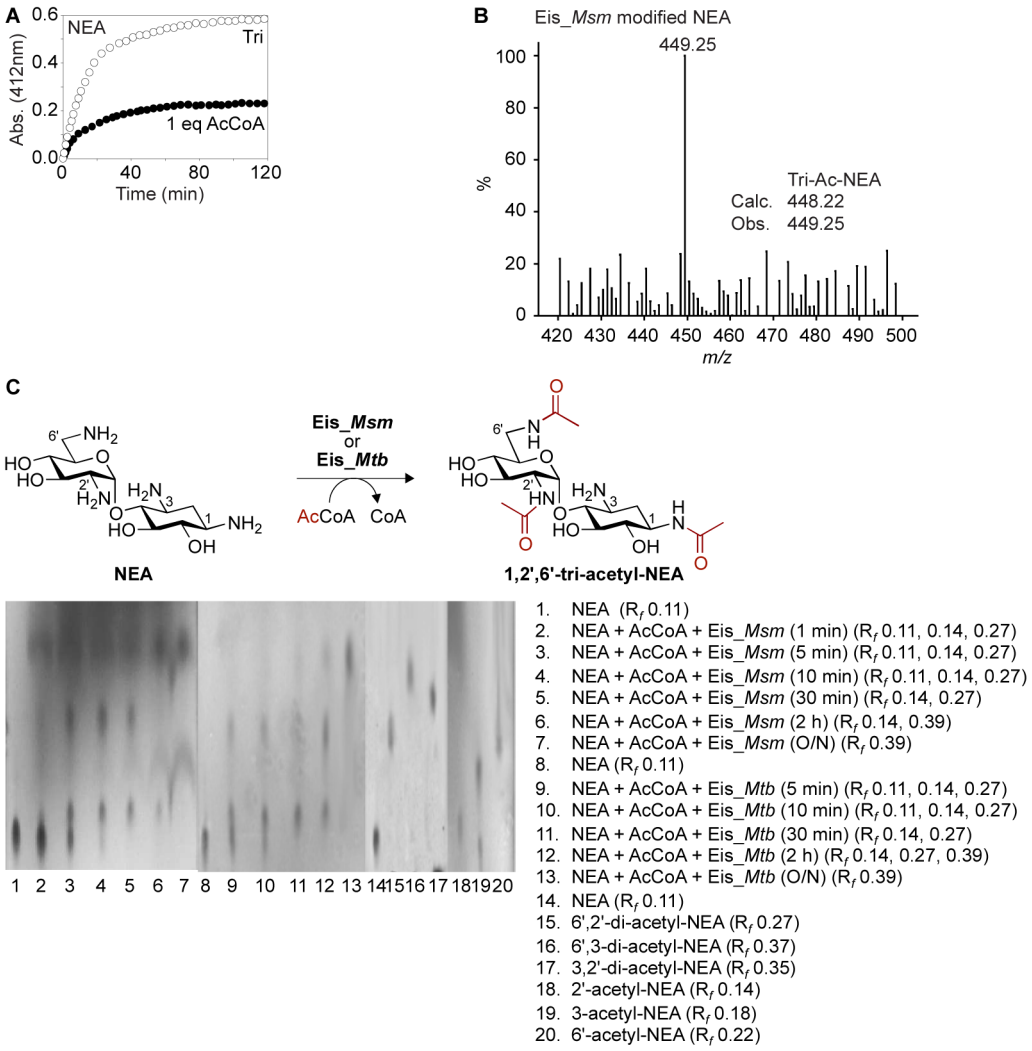

Figure 2.

A. Conversion of NEA into its acetylated products, as monitored by the UV-Vis assay when using Eis_*Msm* with 1 (black circles) and 10 (white circles) equivalents of AcCoA, respectively. **B.** A mass spectrum confirming the formation of tri-acetyl-NEA by Eis_*Msm*. **C.** Multi-acetylation of NEA by Eis_*Msm* observed by the TLC assay. Lanes 1–7: a time course displaying the mono-, di-, and tri-acetyl- NEA products of the Eis_*Msm* reaction. Lanes 8–13: a time course of the NEA reaction with Eis_*Mtb*. Lanes 14–20: Controls for di- and mono-acetylation of NEA performed with AAC(2′)-Ic, AAC(3)-IV, and AAC(6′) sequentially or individually.

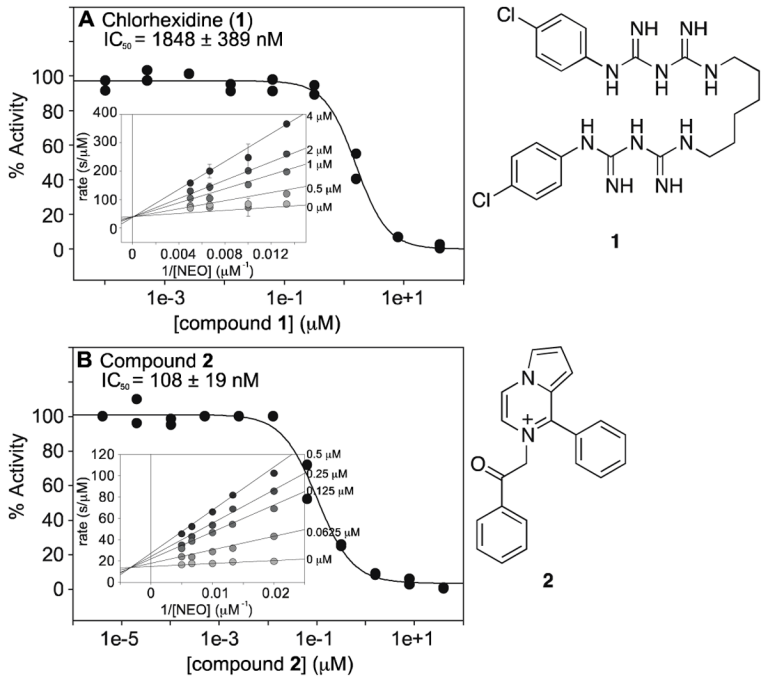

Figure 3.

Inhibition of Eis_*Msm*. IC_{50} curves for **A.** chlorhexidine (**1**), and **B.** compound **2**. The insets show the competitive and mixed inhibition modes of compounds **1** and **2**, respectively.

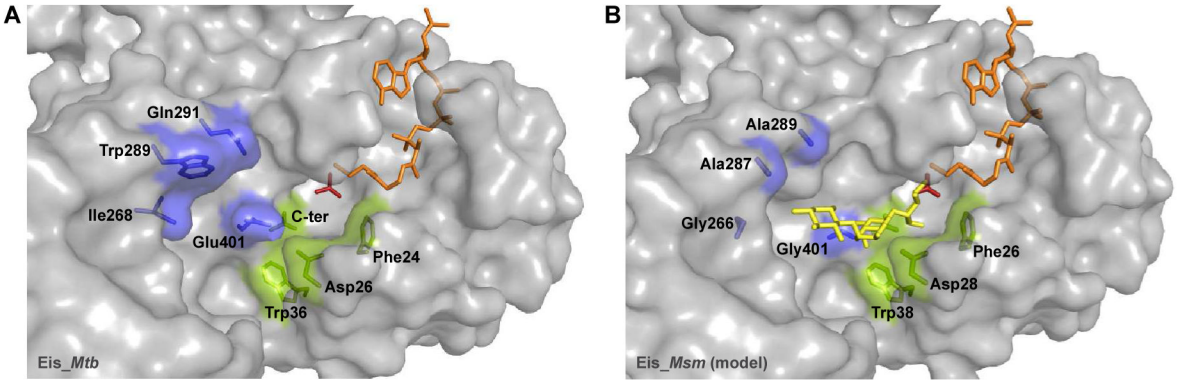

Figure 4.

Structural differences between the AG-binding pockets of Eis_*Mtb* and Eis_*Msm*. **A.** The active site and the AG-binding pocket of Eis_*Mtb* bound to CoA and an acetamide, as seen in the recently reported crystal structure (PDB code: 3R1K (13)). In both panels, CoA is shown in orange, acetamide in red, the conserved AG binding pocket residues in green, and the non-conserved residues in blue. The C-terminal carboxyl group is denoted as C-ter. **B.** A model of the active site and the AG-binding pocket of Eis_*Msm*. This model was generated by substituting the non-conserved residues of the AG-binding pocket Eis_*Mtb* with their Eis_*Msm* counterparts (Ile268, Trp289, and Gln291 in Eis_*Mtb* were mutated to Gly266, Ala287, and Ala289 in the Eis_*Msm* numbering, respectively). As a result of these mutations an APR molecule (in yellow) can be accommodated in the pocket in the orientation appropriate for catalysis. The structure of APR was taken from the high-resolution PDB entry 2OE5.(27)

Table 1

Comparison of level of acetylation by Eis from *M. smegmatis* and *M. tuberculosis*.

AG	*M. smegmatis*	*M. tuberculosis*[a]
AMK	Tri	Tri
APR	Di	×[b]
HYG	Mono	Di
KAN	Di	Di
NEA	Tri	Tri
NEO	Tri	Tri
NET	Di	Di
PAR	Tri	Di
RIB	Tri	Tri
SIS	Tri	Tri
SPT	×	×
STR	×	×
TOB	Tetra	Tetra

[a] We previously reported these data (13).

[b] × indicates that no acetylation was observed.

Table 2

Observed kinetic parameters[a] for [AG]-dependent acetylation by Eis from *M. smegmatis* and *M. tuberculosis*.

	M. smegmatis		M. tuberculosis	
AG	$K_{m,AG}$ (μM)	$k_{cat,AG}$ (s^{-1})	$K_{m,AG}$ (μM)	$k_{cat,AG}$ (s^{-1})
AMK	251 ± 55	0.034 ± 0.003	113 ± 35	0.030 ± 0.004
KAN	278 ± 36	0.108 ± 0.005	490 ± 140	0.12 ± 0.02
NEA	359 ± 101	0.176 ± 0.027	137 ± 57	0.064 ± 0.010
NEO	314 ± 77	0.114 ± 0.014	199 ± 87	0.19 ± 0.04
NET	197 ± 30	0.835 ± 0.057	96 ± 15	0.63 ± 0.03
PAR	153 ± 55	0.035 ± 0.006	96 ± 20	0.15 ± 0.01
SIS	82 ± 8	0.206 ± 0.006	159 ± 48	0.38 ± 0.04
TOB	131± 22	0.267 ± 0.016	116 ± 17	0.21 ± 0.01

[a] All parameters are defined in the Materials and Methods section.

Table 3

Observed kinetic parameters[a] for [AcCoA]-dependent acetylation by Eis from *M. smegmatis* and *M. tuberculosis*.

	M. smegmatis		M. tuberculosis	
AG	$K_{m,AcCoA}$ **(μM)**	$k_{cat,AcCoA}$ **(s^{-1})**	$K_{m,AcCoA}$ **(μM)**	$k_{cat,AcCoA}$ **(s^{-1})**
AMK	58 ± 25	0.142 ± 0.026	8 ± 5	0.015 ± 0.001
KAN	39 ± 17	0.398 ± 0.060	10 ± 3	0.094 ± 0.004
NEA	22 ± 7	0.101 ± 0.008	41 ± 6	0.070 ± 0.004
NEO	76 ± 23	0.546 ± 0.065	32 ± 6	0.116 ± 0.005
NET	108 ± 35	0.819 ± 0.121	124 ± 23	0.36 ± 0.03
SIS	77 ± 19	0.620 ± 0.063	84 ± 11	0.90 ± 0.04

[a] All parameters are defined in the Materials and Methods section.

Table 4

Observed kinetic parameters for KAN acetylation by Eis from *M. smegmatis*.

[AcCoA] (μM)	$K_{m,AG}$ (μM)	$k_{cat,AG}$ (s^{-1})
100	278 ± 36	0.108 ± 0.005
200	450 ± 31	0.18 ± 0.01
500	756 ± 66	0.40 ± 0.02

Table 5

Rate and equilibrium binding constants[a] for the random sequential mechanism of acetylation by Eis from *M. smegmatis* and *M. tuberculosis*.

	M. smegmatis			M. tuberculosis			
AG	$K_{d,AG(E•AcCoA)}$ (μM)	k_{cat} (s^{-1})	$k_{cat}/K_{d,AG(E•CoA)}$ ($s^{-1}M^{-1}$)	$K_{d,AG(E•AcCoA)}$ (μM)	k_{cat} (s^{-1})	$k_{cat}/K_{d,AG(E•CoA)}$ ($s^{-1}M^{-1}$)	$K_{d,AcCoA(E)}$ (μM)[b]
AMK	>1000	>0.3	284 ± 52	32 ± 14	0.016 ± 0.007	500 ± 300	87 ± 23
KAN	2540 ± 160	1.6 ± 0.5	630 ± 200	350 ± 150	0.16 ± 0.07	460 ± 280	
NEA	141 ± 60	0.13 ± 0.05	917 ± 500	95 ± 50	0.08 ± 0.04	870 ± 640	
NEO	>1000	>1.0	1090 ± 130	75 ± 41	0.13 ± 0.07	1800 ± 1400	
NET	108 ± 35	1.0 ± 0.4	7900 ± 4000	31 ± 10	0.4 ± 0.1	12200 ± 5600	
SIS	179 ± 54	0.85 ± 0.25	4700 ± 2050	340 ± 140	1.5 ± 0.6	4500 ± 2600	

[a] All parameters are defined in the Materials and Methods section. Determination of the rest of the equilibrium constants of the mechanism by this method was not reliable due to large propagated uncertainties.

[b] This value is AG-independent and assumed to be the same for Eis_*Msm* and Eis_*Mtb* (see main text) in the calculations of the Eis_*Mtb* parameters in this table.